

GAS ACCRETION IN THE M32 NUCLEUS: PAST & PRESENT

ANIL C. SETH¹

Accepted by ApJ, Oct. 2nd, 2010

ABSTRACT

Using adaptive optics assisted Gemini/NIFS data, I study the present and past gas accretion in the central 3'' of the M32 nucleus. From changes in the spectral slope and CO line depths near the center, I find evidence for unresolved dust emission resulting from BH accretion. With a luminosity of $\sim 2 \times 10^{38}$ ergs⁻¹, this dust emission appears to be the most luminous tracer of current BH accretion, two orders of magnitude more luminous than previously detected X-ray emission. These observations suggest that using high resolution infrared data to search for dust emission may be an effective way to detect other nearby, low luminosity BHs, such as those in globular clusters. I also examine the fossil evidence of gas accretion contained in the kinematics of the stars in the nucleus. The higher-order moments ($h3$ and $h4$) of the line-of-sight velocity distribution show patterns that are remarkably similar to those seen on larger scales in elliptical galaxies and in gas-rich merger simulations. The kinematics suggests the presence of two components in the M32 nucleus, a dominant disk overlying a pressure supported component. I discuss possible formation scenarios for the M32 nucleus in the context of the kinematic data as well as previous stellar population studies. The kinematic measurements presented here are the highest quality available for the nucleus of M32, and may be useful for any future dynamical models of this benchmark system.

Subject headings: galaxies:nuclei – galaxies:active – galaxies: kinematics and dynamics – galaxies:formation – galaxies: individual (M32)

1. INTRODUCTION

The M32 nucleus hosts the smallest of the three supermassive black holes known in the Local Group. Like its counterpart in M31 and the Milky Way, it is currently accreting at very low levels, detectable only due to its proximity. Surrounding the black hole (BH) in M32 is a rotating disk of stars that is the densest stellar system in the local universe. In this paper I use high resolution spectroscopic observations to examine the current accretion of the M32 black hole and study the formation of the stellar nucleus from its present-day kinematics.

The kinematic signature of a supermassive BH at the center of M32 was first recognized by Tonry (1984), and current estimates suggest a BH mass of $2.5 \times 10^6 M_{\odot}$ (Verolme et al. 2002; van den Bosch & de Zeeuw 2010). Accretion onto this BH has been searched for at many wavelengths, but detected only in the X-rays (Ho et al. 2003). The X-ray luminosity from 2-10 keV is 9.4×10^{35} ergs⁻¹, suggesting an accretion rate nine orders of magnitude below the Eddington limit. Like M31 and the Milky Way, the M32 BH presents a rare opportunity to study BH accretion processes at very low levels. In §3, I report detection of hot dust emission from near the black hole at NIR wavelengths with luminosity exceeding the X-ray luminosity by two orders of magnitude.

In the second half of the paper (§4), I use the kinematics of the nuclear region to constrain the formation history of its stars. The formation history of stars in the immediate vicinity of the BH is likely to be connected in some way to the formation of the BH itself (e.g. Hopkins & Quataert 2010b). The nucleus of M32 contains a rotating disk of stars that reaches a den-

sity at $r < 0.1$ pc of $>10^7 M_{\odot}/\text{pc}^{-3}$, making it the densest stellar system known (Walker 1962; Lauer et al. 1998). Morphologically, the nuclear component appears to be distinct from the rest of the galaxy, with the surface brightness profile showing evidence for an additional stellar component at radii $<5''$ (20 pc) (Kormendy 1999; Graham & Spitler 2009). This component has an effective radius of $1.5''$, and an I band luminosity of $\sim 3 \times 10^7 M_{\odot}$ (Graham & Spitler 2009), $\sim 10\%$ of the total galaxy luminosity (see also Kormendy et al. 2009). The mass and size typical of this component is typical of nuclear star clusters commonly seen at the centers of lower luminosity early-type galaxies, but it contains a much larger fraction of the total galaxy luminosity than usual (e.g. Côté et al. 2006).

Despite the evidence for a morphologically distinct component in the central $5''$, no corresponding separation is seen in the stellar populations or kinematics. The rotation velocity decreases slowly with radius (Dressler & Richstone 1988) but there is no break suggesting a separation between the nuclear disk and the rest of the galaxy. The stellar populations of the nucleus are younger, than the galaxy as a whole, with an average age of ~ 4 Gyr in the nucleus rising to ~ 8 Gyr at larger radii (Worthey 2004; Rose et al. 2005; Coelho et al. 2009). However, again there is no evidence for a break in the stellar population properties as a function of radius. In §4 I show that there is a kinematic signature in the nucleus that is remarkably similar to merger simulations done at larger scales. This signature provides strong evidence for a two component system in the M32 nucleus, with a dominant disk component embedded in a pressure-supported component. I outline a scenario, in which the nuclear disk formed gradually from the stellar winds of stars in the bulge of M32, that may provide a good ex-

¹Harvard-Smithsonian Center for Astrophysics, 60 Garden Street Cambridge, MA 02138, *OIR Postdoctoral Fellow*

planation of the observed kinematics, stellar populations and abundance gradients seen in the nucleus.

2. DATA

Integral field spectra of the central $3'' \times 3''$ of M32 were obtained with Gemini NIFS on Oct 23, 2005. A total of 11×600 s K band exposures were taken, with 6 on source and 5 offset to a blank sky position. The nucleus was used as a natural guide star to obtain an adaptive optics correction with the ALTAIR system. Two previous papers have utilized this same dataset (Davidge et al. 2008, 2010) but were restricted to the study of stellar populations in the nucleus.

Data were obtained from the Gemini Science Archive and reduced following the same process outlined in Seth et al. (2008) and Seth et al. (2010). An A0V star, HIP 116449, was used as a telluric calibrator. This star was also used for photometric and spectrophotometric calibration, both of which have errors of $\sim 10\%$. Wavelength calibration utilized both an arc lamp image and the sky lines in the spectrum, and has an absolute error of $\sim 2 \text{ km s}^{-1}$. The median spectral resolution was 4.2 \AA (57 km s^{-1}) FWHM. The signal-to-noise ratio of the spectrum is very high, ranging from 280 per $0''.05'' \times 0''.05$ pixel in the center to 60 in the corner of the field ($r = 2''.1$).

To determine the point spread function (PSF) of the observations I followed a two-step process similar to that described in Seth et al. (2010). I assumed a PSF described by an inner Gaussian core + outer Moffat halo (with the Moffat function described as $\Sigma(r) = \Sigma_0 / [(1 + (r/r_d)^2)^{4.765}]$). I used the observation of the telluric calibrator to measure the outer halo of the PSF and found a best fit $r_d = 0''.83$ containing 55% of the light. I then fixed this outer halo, and fit the inner part of the galaxy PSF by convolving an HST image of M32 to fit our NIFS image (after making a minor correction for the dust emission, see §3 for details). For the HST image, I used an F1042M WFPC2 image where the nucleus was located on the planetary camera. I found a very good fit to the NIFS image by convolving this HST image using an inner Gaussian with FWHM of $0''.25$ and containing 45% of the light (along with the outer Moffat with $r_d = 0''.83$); typical fit residuals were 4%. The compact dust emission discussed in the next section has a FWHM of $0''.25$, an independent confirmation of the PSF core width. Measurements of the CO bandhead strength used in §3 and plotted in Fig. 1 were made in each spaxel after dividing by the telluric star spectrum using the $^{12}\text{CO}(2,0)$ index defined by Kleinmann & Hall (1986).

I derived kinematics from the NIFS data from the CO bandhead between $2.28 \mu\text{m}$ and $2.395 \mu\text{m}$ using the penalized-pixel fitting (PPXF) method of Cappellari & Emsellem (2004) to determine the line-of-sight velocity distribution (LOSVD). The program parameterizes the LOSVD using the radial velocity (V), dispersion (σ), skewness ($h3$) and kurtosis ($h4$). High resolution templates from Wallace & Hinkle (1996) were used and convolved to the spectral resolution of each pixel as determined from sky lines (see Seth et al. 2010, for more details).

The measurements presented here are the highest quality kinematic data available that resolves the sphere-of-influence of the BH. The very high S/N results in

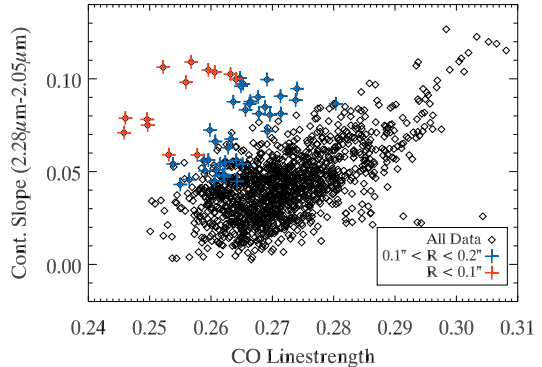


FIG. 1.— The CO line strength plotted against continuum slope. Positive values indicate deeper CO lines and redder continuum slopes. Spaxels between $0''.1$ and $0''.2$ of the center are shown with blue crosses, and those within $0''.1$ with red crosses. The deviation towards redder colors and weaker CO lines is due to emission from hot dust. The slope is measured from the flux ratioed spectra, thus a value of zero indicates the same spectral slope as an A0 star. Errors on the CO depths are $\lesssim 0.005$ and on the continuum slopes, $\lesssim 0.0002$.

errors on the LOSVD that are much smaller than for the HST/STIS measurements presented by Joseph et al. (2001). The spatial resolution of the NIFS observations is somewhat lower than with STIS, but NIFS provides integral field coverage that can help significantly in constraining dynamical models (e.g. Shapiro et al. 2006; Neumayer et al. 2007; Nowak et al. 2008). Our kinematic measurements are consistent with those of Joseph et al. (2001) except in the central few tenths of an arcsecond, where the higher resolution of STIS results in a steeper velocity gradient and a central dispersion higher by $\sim 10\%$. As M32 is a benchmark for studies of BH mass measurements and dynamics codes (van der Marel et al. 1998; Verolme et al. 2002; Kormendy 2004; van den Bosch & de Zeeuw 2010), I make the full kinematic data set available in Table 1 for use in future studies.

3. HOT DUST: THE MOST LUMINOUS TRACER OF CURRENT BH ACCRETION

The spectral energy distributions (SEDs) of quasar and Seyfert nuclei in the K band are typically dominated by hot dust with temperatures of 800-1500 K (e.g. Kobayashi et al. 1993; Alonso-Herrero et al. 1996; Winge et al. 2000; Riffel et al. 2009). High resolution observations with HST NICMOS and adaptive optics observations have shown that these sources are typically unresolved, and thus originate quite close to the accreting BH (Quillen et al. 2001; Riffel et al. 2010). From measurements of the time-lag between UV and NIR light, the size of this dust-emitting region has been constrained to be $\ll 1$ pc in nearby Seyfert galaxies (Minezaki et al. 2004, 2006). The luminosity of the dust emission correlates strongly with AGN luminosities at other wavelengths (Quillen et al. 2001). Recently, we found unresolved and possibly variable hot dust emission in the nucleus of the nearby S0 galaxy NGC 404 (Seth et al. 2010), the first detection of compact dust emission in a low-luminosity (LINER) AGN.

The presence of dust emission in the nucleus of M32 is inferred due to the presence of a redder continuum and weaker CO lines in the central $0''.2$. This is shown

TABLE 1
GEMINI/NIFS KINEMATIC DATA OF THE M32 NUCLEUS

$\Delta\alpha$ ["]	$\Delta\delta$ ["]	V_r [km s ⁻¹]	σ [km s ⁻¹]	$h3$	$h4$
0.014	-0.015	-206.14±1.08	117.94±1.23	0.018±0.007	0.038±0.007
0.014	0.035	-215.93±1.09	114.63±1.17	0.022±0.007	0.053±0.007
-0.036	-0.015	-208.52±1.10	115.40±0.87	0.022±0.005	0.043±0.007

(See *Online Journal Article for Full Data Table*)

in Fig. 1. Typically, the color of the continuum correlates with the depth of the CO line as cooler redder stars have deeper CO lines. However, within the central 0''.2, (and especially the central 0''.1 shown with red crosses in Fig. 1), the continuum gets redder while the CO lines become weaker indicating the presence of hot dust emission. To determine the contribution from this hot dust component I fit the M32 nuclear spectrum to a combination of a blackbody model and an annular spectrum from radii of 0''.5-1'' (as in Fig. 4 of Seth et al. 2010). The best fitting temperature for the dust at the center ($r < 0''.1$) is 920K. The residuals of the fit are 1.1%, a factor of two improvement over a fit with no dust.

I fit the dust contribution to each spaxel in the data cube fixing the dust temperature to 920K. Dust emission is only found at $r \lesssim 0''.2$ and reaches a maximum contribution of ~5% of the total light. The dust emission is unresolved, with a FWHM of 0''.25 matching the NIFS PSF derived from HST observation. The emitting region is therefore constrained to be <0.9 pc.

The total flux of the hot dust emission from 2.0-2.43 μm is $1.7 \times 10^{-13} \text{ erg s}^{-1} \text{ cm}^{-2}$ corresponding to a luminosity in the K band of $1.2 \times 10^{37} \text{ erg s}^{-1}$. Integrating over the full Planck function, the total luminosity is $1.8 \times 10^{38} \text{ erg s}^{-1}$. The corresponding K band magnitude of the emission is $K=15.0$ ($M_K = -9.4$). The primary uncertainty in these flux and luminosity measurements is the temperature of the dust, which is not well constrained by our fits. Taking a reasonable range of temperatures from 800-1300K, the flux ranges from $1.5\text{-}2.5 \times 10^{-13} \text{ erg s}^{-1} \text{ cm}^{-2}$, the K band luminosity from $1.0\text{-}1.7 \times 10^{37} \text{ erg s}^{-1}$ and the total luminosity from $1.3\text{-}2.6 \times 10^{38} \text{ erg s}^{-1}$.

The weaker CO lines and redder continuum cannot result just from changes in the stellar population at the center of M32. There is little indication of any change in the optical and UV colors near the center of M32, although slightly bluer colors are seen in the central pixels of a WFPC2 F555W-F814W color image by Lauer et al. (1998). The Galactic center also shows a decrease in CO line depth within the central parsec (Sellgren et al. 1990) which likely results from the decrease in the fraction of light coming from late-type stars in the central parsec (Genzel et al. 1996; Do et al. 2009; Bartko et al. 2010). This decrease may be caused by stellar collisions preferentially destroying the larger radius RGB and AGB stars (e.g. Dale et al. 2009). The M32 stellar density is sufficient that such collisions may occur there as well (Lauer et al. 1998). However, this mechanism cannot by itself explain the effect shown in Fig. 1, as the removal of larger radius RGB and AGB stars would make K band continuum bluer, not redder.

Emission from hot dust could also result from heating by the stellar component. M32 has a population of post-

AGB and extreme Horizontal Branch stars (Brown et al. 1998, 2000), but these are much less compactly distributed than the dust emission. Furthermore, the total UV luminosity at 1600Å is insufficient to heat the dust ($\nu L_\nu \sim 2 \times 10^{37} \text{ erg s}^{-1}$; Cole et al. 1998), and the UV-to-optical colors do not decrease at the center of M32 (Lauer et al. 1998). Therefore hot stars do not appear to be responsible for the dust emission. The interacting stellar winds resulting from the high stellar density and velocity dispersion could also provide energy to heat the dust. The conditions at the center of M32 are fairly similar to those in the MW center where no comparable hot dust component is seen. However, there is a significant warm dust component in the Milky Way center with $T \sim 400$ K and luminosity of order $10^{38} \text{ erg s}^{-1}$ within the central parsec (Zylka et al. 1995; Stolovy et al. 1996; Mezger et al. 1996). I also note that there are no signatures of compact hot dust emission in NIFS observations of local group galaxies M33 and NGC 205 which also have high stellar densities (but lower dispersions). Based on the lack of hot dust emission in these systems, I argue that the hot dust in the nucleus of M32 is likely powered by BH accretion.

The compact hot dust emission appears to be the most luminous BH accretion signature observed in the M32 nucleus. Ho et al. (2003) analyzed a variety of radio and X-ray data and detect the nucleus only in X-rays, with a 2-10 keV luminosity of $9.4 \times 10^{35} \text{ erg s}^{-1}$. Based on this X-ray luminosity and the expected supply of gas available for accretion Ho et al. (2003) found that the radiative or BH accretion efficiency must be very small ($\lesssim 10^{-3}$). Such low efficiencies are found in radiatively inefficient accretion models (e.g. Quataert 2001; Ho 2009). The NIR emission discussed here would allow for a somewhat higher accretion efficiency, but still likely lower than the 10% efficiency of a canonical accretion disk. This suggests that strong NIR dust emission may be found in lower accretion states as well as the higher accretion states where they have traditionally been observed. The dust emission in Seyferts and quasars is thought to come from a radiatively heated sublimation zone in the accretion disk or at the inner edge of the torus. However, the excitation mechanism for the hot dust emission in M32 is unclear. The NIR luminosity derived here is two orders of magnitude brighter than the observed X-ray luminosity found by Ho et al. (2003). In studies of other low luminosity AGN, the NIR to X-ray luminosity ratios are typically unity (Ho 1999, 2008; Eracleous et al. 2010). These systems are somewhat higher luminosity systems than M32, but all are expected to be radiatively inefficient accretors with similar spectral energy distributions (Ho 2009). Furthermore, the observed X-ray luminosity and UV upper limits (Cole et al. 1998; Ho et al. 2003) are insufficient to supply the radiative energy needed to

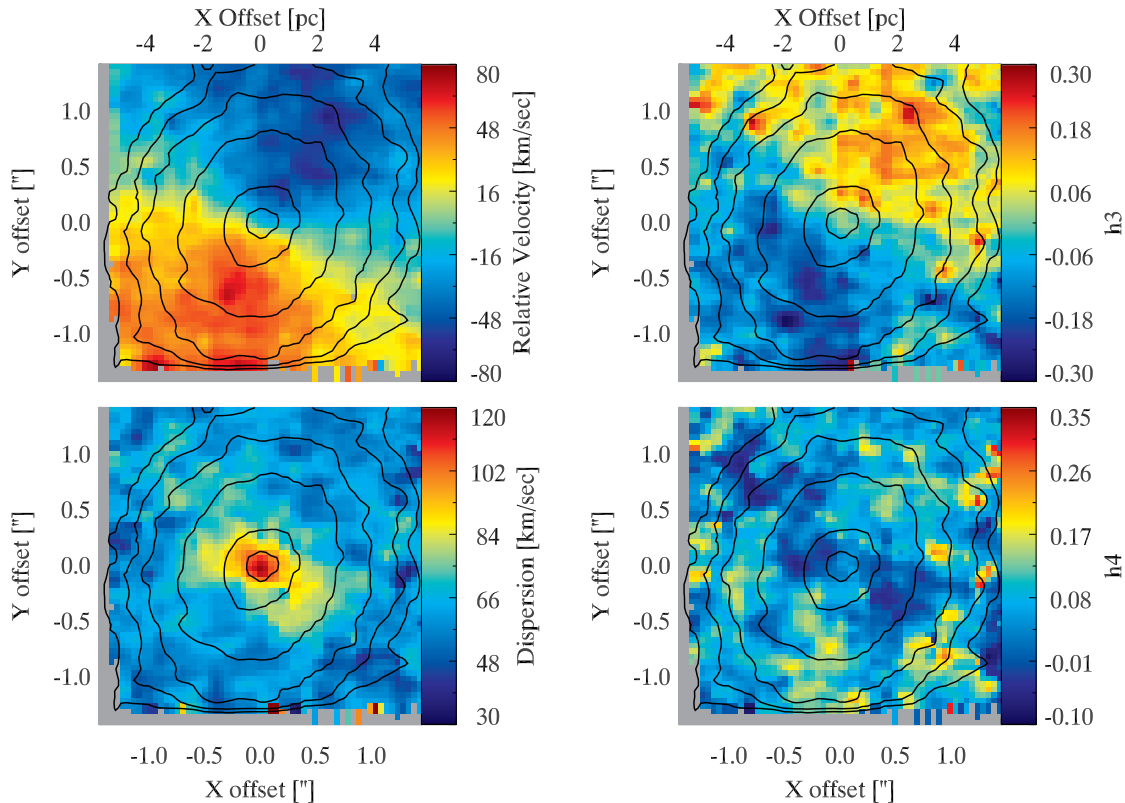


FIG. 2.— The line-of-sight velocity distribution of M32 derived from the Gemini/NIFS data at the CO bandhead ($2.3\mu\text{m}$). The radial velocity is shown in the top left panel after removal of the systemic velocity of -200 km s^{-1} . The bottom left panel shows the dispersion, the top right the skewness or $h3$ component, and the bottom right the kurtosis or $h4$ component of the LOSVD. These data are the highest S/N data available of the M32 nucleus that resolve the BH sphere of influence.

heat the dust. Both these problems could be solved if the BH accretion in M32 is significantly time variable, with our observations taken at a time when there was higher flux at all wavelengths. Alternatively, the heating of the hot dust could result from mechanical feedback from the BH (e.g. Clénet et al. 2005) or possibly stellar winds as discussed above.

Based on the limited examples of M32 and NGC 404 (Seth et al. 2010), it appears NIR spectra at high spatial resolution may be an effective way to search for accretion in the lowest luminosity AGN. In both these cases, the NIR emission is the most luminous activity tracer, more luminous than the detected X-ray emission. Furthermore, the low luminosity of the X-ray emission ($\lesssim 10^{38}\text{ erg s}^{-1}$) can be confused with emission from X-ray binaries (e.g. Desroches & Ho 2009; Gallo et al. 2010) and thus the NIR emission may represent the best indicator of BH accretion if it can be spectrally disentangled from the stellar light. One very interesting application of this technique would be to search for hot dust emission from accreting BHs in G1 and other globular clusters with putative central BHs (e.g. Ulvestad et al. 2007; Noyola et al. 2010).

4. A KINEMATIC SIGNATURE OF PAST GAS ACCRETION

In this section I discuss kinematic measurements from the CO bandhead of the NIFS data. The higher-order moments of the LOSVD show a very clear signature similar to that typically seen on larger scales in kinematic measurements of the centers of rotating, disk elliptical

galaxies (e.g. Bender et al. 1994; Krajnović et al. 2008). The kinematic signature seen in these galaxies has been recently been simulated as resulting from gas accretion at the centers of galaxies during the end phases of gas-rich major mergers (Hoffman et al. 2009, 2010). I analyze these kinematic results in light of these observations and simulations.

Maps of the first four moments of the LOSVD derived from our NIFS data are shown in Fig. 2. The velocity map shows strong rotation at a position angle of -25° (E of N) with an amplitude of $\sim 55\text{ km s}^{-1}$ beyond a radius of $0''.3$ (derived using the kinemetry software of Krajnović et al. 2006). The dispersion increases to a maximum of 120 km s^{-1} in the central $0''.5$ due to the influence of the BH and unresolved rotation; outside of this radius, it drops to values of $\sim 60\text{ km s}^{-1}$. The $h3$ distribution is clearly anti-correlated with the velocity, while a more complex but axially symmetric pattern is visible in the $h4$ map with negative values along the minor axis and strong positive values along the major axis. The effect of individual stars is clearly seen in the outer parts of the kinematic maps; these result in lower dispersions, extreme $h3$ values and strongly positive $h4$ values. The properties of these stars are discussed in Davidge et al. (2010).

The top panels of Figure 3 shows the $h3-v/\sigma$ and $h4-v/\sigma$ distributions of the data. The $h3$ distribution is strongly and tightly anti-correlated with v/σ . The highest $h4$ values are found in the most strongly

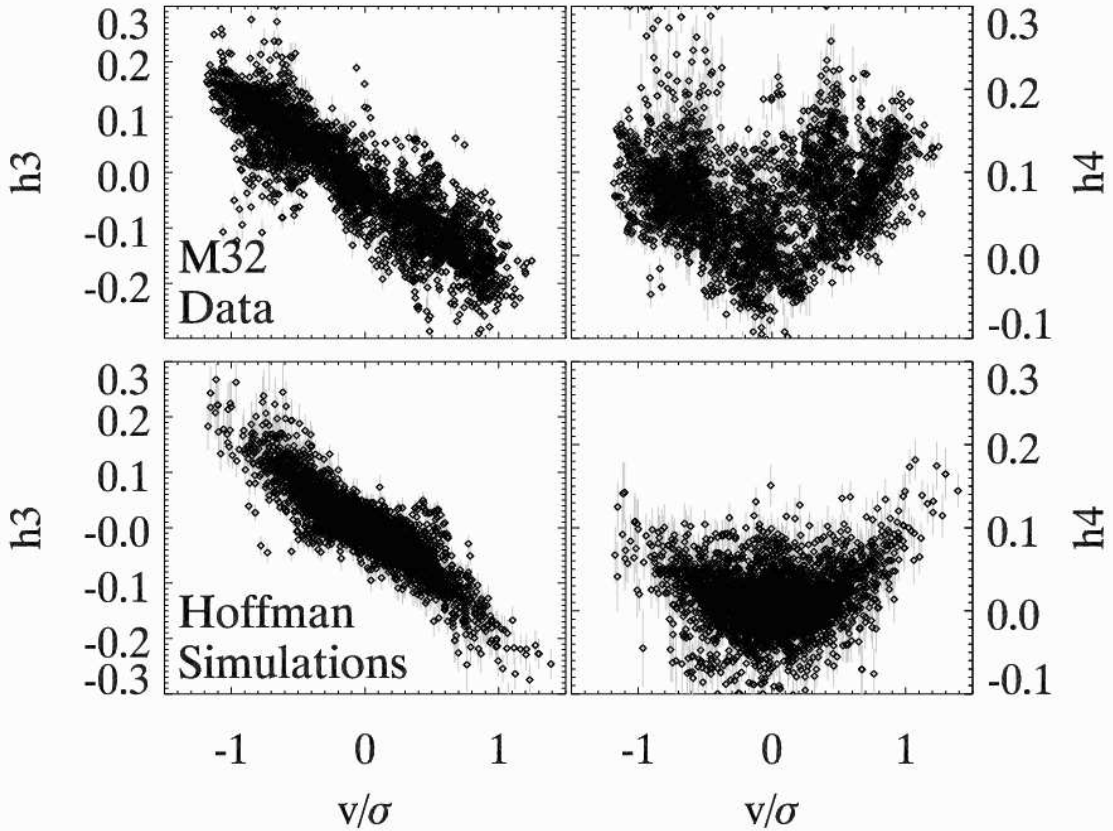


FIG. 3.— Distribution of the higher order LOSVD moments (h_3 and h_4) as a function of the rotation velocity divided by the dispersion V/σ at $r < 1.5''$. The top panels display the Gemini/NIFS kinematics of M32, while the bottom panels display data from gas-rich mergers at similar orientations by Hoffman et al. (2009). In the top panels, each spaxel in our IFU observations is plotted as a single data point (with a light gray error bar), while the simulation data has been analyzed in a similar way to mimic IFU data.

rotating regions of the M32 nucleus. Both the h_3 and h_4 trends are remarkably similar to those seen on larger kiloparsec scales in observations (Bender et al. 1994; Krajnović et al. 2008) and in recent simulations (Hoffman et al. 2009). The h_3 anti-correlation with v/σ is naturally explained by the presence of some stars centered at the systemic velocity, while the positive h_4 values can also result from the superposition of a cold disk and hot bulge or be a signature of violent relaxation. In combination, these trends suggest the presence of two coincident components in the M32 nucleus, a dominant rotating disk and a thermalized, relaxed bulge structure.

To facilitate visual comparison between our observations and the simulations, in the bottom panels of Figure 3 I have plotted models from Hoffman et al. (2009). The plotted models are the results of 8 gas-rich (40% gas), equal mass mergers. The kinematic data was derived by viewing the central few kiloparsecs of these simulations from a variety of lines-of-sight with inclinations consistent with the $70 \pm 5^\circ$ inclination for the central disk of M32 found by Verolme et al. (2002). The slope and extent of the h_3 - v/σ distribution is almost identical to that seen in the simulations. For h_4 , both the simulations and data have generally positive h_4 with a strong similarity in the shapes of the h_4 - v/σ distribution. The very high h_4 (> 0.15) values seen in the M32 data are the result of individual stars and clumps super-imposed on the velocity field.

The kinematic data provide evidence for a two component system including a disk created by gas accretion into the nucleus. However, the details of the gas accretion leading to the formation of the central disk may be somewhat different than in the simulations due to the large differences in scale between them. Embedded disk structures occur in the Hoffman et al. (2009) simulations only in gas-rich major mergers and form on short timescales. However on the smaller scales of the M32 nucleus, it is possible that lower gas fraction mergers, gas-rich minor mergers, or even secular processes are still capable of creating the disky kinematics seen in M32 on parsec scales. For instance, in Seth et al. (2010), we present evidence that a minor merger ~ 1 Gyr ago in NGC 404 appears to be responsible for a burst of star formation that formed ~ 5 million solar masses of stars in the central 10 pc of that S0 galaxy.

Another possibility for formation of nuclear disk is the gradual accretion of material from stellar winds at the center of the galaxy as described by Bailey (1980). This would naturally lead to a gradual trend in stellar age (Worthey 2004; Rose et al. 2005) and the lack of any break in the rotation curve (Dressler & Richstone 1988). Furthermore, this scenario may naturally account for the abundance gradient in the nucleus; Worthey (2004) and Rose et al. (2005) find the $[\text{Mg}/\text{Fe}]$ ratio is significantly subsolar in the nucleus and increases with increasing radius. If the stars in the nucleus were made from the

stellar winds of previous generations of stars, then this might result in a drop in the $[\text{Mg}/\text{Fe}]$ (e.g. as in the Milky Way globular cluster NGC 2808; Carretta et al. 2009). There is sufficient mass in the bulge of M32 to supply the necessary gas to the nucleus. However, whether the gas would actually end up as a rotating structure at the center would require detailed hydrodynamic simulations. This scenario could also be tested using stellar population modeling of resolved stars and spectra in and around the nucleus if the models are accurate enough to distinguish between populations of intermediate (2-10 Gyr) age (e.g. Marigo et al. 2008).

4.1. Asymmetries in the M32 Nucleus

Simulations by Hopkins & Quataert (2010a,b) follow gas accretion down to parsec scales in galaxy mergers and find that gas accretion in the presence of BHs cause the formation of lopsided disks. These disks correspond quite well to the eccentric disk seen in M31 (e.g. Lauer et al. 1993), and Hopkins & Quataert (2010b) suggest that this disk formed at the same time the M31 BH was growing. Due to the parsec scale of the expected asymmetries, M32 is one of the few other galaxies close enough for the asymmetries to be seen. If the M32 nucleus had a major merger formation scenario similar to that considered by Hopkins & Quataert (2010b), a lopsided nuclear disk would be expected. While M32 clearly does not have the prominent asymmetric structure similar to that seen at the center of M31, I analyzed HST images to see if there is any evidence for a lower level asymmetry.

Archival HST WFPC2/PC images were obtained in four bands (F336W, F555W, F675W, and F814W) from the CADZ WFPC2 associations². I then fit axially symmetric model profiles to the data, subtracted these off and examined the residuals. Fits to the images in each filter were performed on the central $20''$ of each image using elliptical double Sérsic profiles. The outer Sérsic component was constrained to have the same indices and effective radii as fits to the 1-D M32 surface-brightness profile by Graham (2002) and Graham & Spitler (2009) that include measurements from the same F814W HST data we use here. All fits were convolved with an appropriate TinyTim WFPC2 PSF (Krist 1995). The resulting fits accurately described the light profile at all radii to within 3%. The inner Sérsic profile fits had effective radii of 1.5-1.6'', consistent with that found by Graham & Spitler (2009), minor-to-major axis ratios of 0.73 and position angles of -20° . After subtraction of these profiles, some asymmetric residuals were visible (see Fig. 4, left panel). To quantify these, I compared the total residual flux on one side of the minor axis to the other in elliptical annuli (Fig. 4, right panel). At radii between $0''.45$ and $1''.8$ ($\sim 2-7$ pc) there is an excess of 1-2% of the total flux in the southern half relative to the northern half. This is seen most clearly in F555W and F675W, and is also present but less clear in the other two bands due to lower S/N (at F336W) and increased surface brightness fluctuations (in F814W).

This small photometric asymmetry is much less lopsided than the central part of M31 (where the disk eccentricity $\sim 40\%$). The asymmetry corresponds to a total mass of $\sim 4 \times 10^5 M_\odot$ derived from the F814W band using

the mass-to-light ratio from Verolme et al. (2002). It is unclear if such small asymmetries are consistent with the Hopkins & Quataert (2010b) model. The physical situation in M32 is quite different from M31, with a much smaller BH mass and a higher stellar density. Simulations that are more appropriate to M32 may serve to both (1) help understand in detail how the M32 nucleus formed, and (2) test the feasibility of the lopsided disk model for driving BH growth in lower mass systems.

5. CONCLUSIONS

In this paper, I have presented results on the current and past gas accretion in the M32 nucleus using adaptive optics assisted Gemini/NIFS data. The data reveal an unresolved emission component at the center of M32 that results in the weakening of CO lines and reddening of the continuum slope in the nucleus. This emission appears to originate from hot dust emission close to the BH as seen in many higher luminosity AGN. The hot dust emission is unresolved with a size of < 0.9 pc and has a luminosity of $\sim 2 \times 10^{38}$ erg s⁻¹. This luminosity is more than two orders of magnitude more luminous than the X-ray emission detected from the central BH by Ho et al. (2003), the only other bandpass in which emission due to accretion has been detected in this galaxy. Combined with similar emission in the nearby low luminosity LINER NGC 404, this suggests that high resolution NIR spectra may be an efficient way of locating low level activity from BHs in nearby galaxies and globular clusters.

I also present the highest quality kinematics of the M32 nucleus currently available, potentially useful for any future dynamical studies of this benchmark system. These measurements cover the central $3'' \times 3''$ with a resolution of $0''.25$. The very high signal-to-noise of these measurements allows accurate determination of the higher order moments which reveal a remarkable kinematic signature similar to those seen on larger scales in elliptical galaxies and merger simulations. The signature manifests as an anti-correlation of $h3$ with v/σ and strongly positive $h4$ especially in areas of strong rotation. These kinematics suggest the presence of a dominant disk component embedded in a pressure supported system. I propose a possible formation scenario in which the M32 nucleus forms from stellar winds of the M32 bulge. This scenario qualitatively explains the kinematic, stellar population and abundance properties of the nucleus. I also briefly consider whether M32 contains any asymmetries in its nucleus, as might be expected based on the Hopkins & Quataert (2010b) simulations of major mergers. A small $\sim 2\%$ photometric asymmetry is found at radii between 2 and 7 pc.

Acknowledgments: The author would like to thank the referee, Luis Ho, for improving this paper. He also thanks Loren Hoffman for sharing her simulation data, and to thank her, Michele Cappellari, Davor Krajnović, Jay Strader, Nelson Caldwell, Knut Olsen, Hagai Perets, and Margaret Geller for helpful discussions. The author is supported by a fellowship from the Smithsonian Institute.

Facilities: Gemini:Gillett (NIFS/ALTAIR), HST (WFPC2)

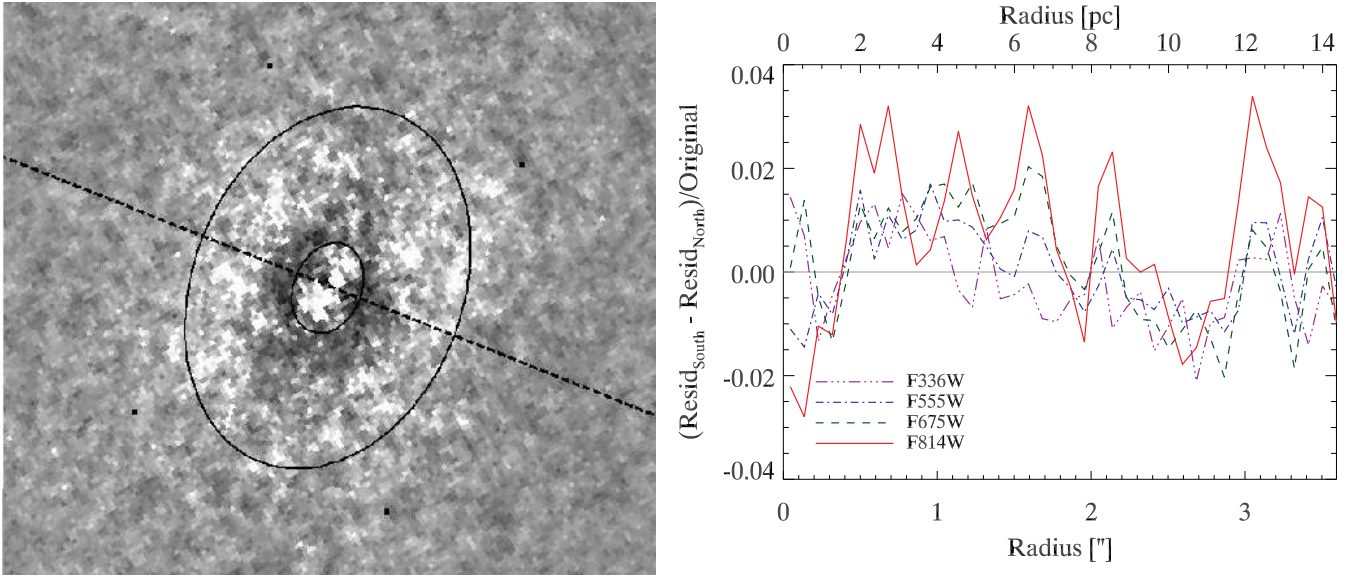


FIG. 4.— Figures showing a small asymmetry in the M32 nucleus. *Left* – shows the a model-subtracted F555W image oriented with N up and E to the left. Black solid lines show the annulus with major-axes of $0.45''$ to $1.8''$, while the dashed line separates the northern and southern halves of this annulus. *Right* – comparison of the residuals of the model-subtracted images. The Y-axis plots the difference in flux between the southern and northern annuli in the model-subtracted images normalized by the original image. A 1-2% excess in the southern annulus is seen in all bands from 0.45 – $1.8''$ (2 – 7 pc).

REFERENCES

- Alonso-Herrero, A., Ward, M. J., & Kotilainen, J. K. 1996, *MNRAS*, 278, 902
- Bailey, M. E. 1980, *MNRAS*, 191, 195
- Bartko, H. et al. 2010, *ApJ*, 708, 834
- Bender, R., Saglia, R. P., & Gerhard, O. E. 1994, *MNRAS*, 269, 785
- Brown, T. M., Bowers, C. W., Kimble, R. A., Sweigart, A. V., & Ferguson, H. C. 2000, *ApJ*, 532, 308
- Brown, T. M., Ferguson, H. C., Stanford, S. A., & Deharveng, J. 1998, *ApJ*, 504, 113
- Cappellari, M., & Emsellem, E. 2004, *PASP*, 116, 138
- Carretta, E., Bragaglia, A., Gratton, R., & Lucatello, S. 2009, *A&A*, 505, 139
- Clénet, Y., Rouan, D., Gratadour, D., Marco, O., Léna, P., Ageorges, N., & Gendron, E. 2005, *A&A*, 439, L9
- Coelho, P., Mendes de Oliveira, C., & Fernandes, R. C. 2009, *MNRAS*, 396, 624
- Cole, A. A. et al. 1998, *ApJ*, 505, 230
- Côté, P. et al. 2006, *ApJS*, 165, 57
- Dale, J. E., Davies, M. B., Church, R. P., & Freitag, M. 2009, *MNRAS*, 393, 1016
- Davidge, T. J., Beck, T. L., & McGregor, P. J. 2008, *ApJ*, 677, 238
- 2010, *PASP*, 122, 241
- Desroches, L.-B., & Ho, L. C. 2009, *Astrophysical Journal*, 690, 267
- Do, T., Ghez, A. M., Morris, M. R., Lu, J. R., Matthews, K., Yelda, S., & Larkin, J. 2009, *ApJ*, 703, 1323
- Dressler, A., & Richstone, D. O. 1988, *ApJ*, 324, 701
- Eracleous, M., Hwang, J. A., & Flohic, H. M. L. G. 2010, *ApJS*, 187, 135
- Gallo, E., Treu, T., Marshall, P. J., Woo, J., Leipski, C., & Antonucci, R. 2010, *ApJ*, 714, 25
- Genzel, R., Thatte, N., Krabbe, A., Kroker, H., & Tacconi-Garman, L. E. 1996, *ApJ*, 472, 153
- Graham, A. W. 2002, *ApJ*, 568, L13
- Graham, A. W., & Spitler, L. R. 2009, *MNRAS*, 397, 2148
- Ho, L. C. 1999, *ApJ*, 516, 672
- 2008, *ARA&A*, 46, 475
- 2009, *ApJ*, 699, 626
- Ho, L. C., Terashima, Y., & Ulvestad, J. S. 2003, *ApJ*, 589, 783
- Hoffman, L., Cox, T. J., Dutta, S., & Hernquist, L. 2009, *ApJ*, 705, 920
- 2010, arXiv:1001.0799
- Hopkins, P. F., & Quataert, E. 2010a, *MNRAS*, 1085
- 2010b, *MNRAS*, 405, L41
- Joseph, C. L. et al. 2001, *ApJ*, 550, 668
- Kleinmann, S. G., & Hall, D. N. B. 1986, *ApJS*, 62, 501
- Kobayashi, Y., Sato, S., Yamashita, T., Shiba, H., & Takami, H. 1993, *ApJ*, 404, 94
- Kormendy, J. 1999, in *Astronomical Society of the Pacific Conference Series*, Vol. 182, *Galaxy Dynamics - A Rutgers Symposium*, ed. D. R. Merritt, M. Valluri, & J. A. Sellwood, 124+–
- Kormendy, J. 2004, in *Coevolution of Black Holes and Galaxies*, ed. L. C. Ho, 1+–
- Kormendy, J., Fisher, D. B., Cornell, M. E., & Bender, R. 2009, *ApJS*, 182, 216
- Krajinović, D. et al. 2008, *MNRAS*, 390, 93
- Krajinović, D., Cappellari, M., de Zeeuw, P. T., & Copin, Y. 2006, *MNRAS*, 366, 787
- Krist, J. 1995, in *ASP Conf. Ser. 77: Astronomical Data Analysis Software and Systems IV*, 349+–
- Lauer, T. R., Faber, S. M., Ajhar, E. A., Grillmair, C. J., & Scowen, P. A. 1998, *AJ*, 116, 2263
- Lauer, T. R. et al. 1993, *AJ*, 106, 1436
- Marigo, P., Girardi, L., Bressan, A., Groenewegen, M. A. T., Silva, L., & Granato, G. L. 2008, *A&A*, 482, 883
- Mezger, P. G., Duschl, W. J., & Zylka, R. 1996, *A&A Rev.*, 7, 289
- Minezaki, T., Yoshii, Y., Kobayashi, Y., Enya, K., Suganuma, M., Tomita, H., Aoki, T., & Peterson, B. A. 2004, *ApJ*, 600, L35
- Minezaki, T. et al. 2006, *ApJ*, 643, L5
- Neumayer, N., Cappellari, M., Reunanen, J., Rix, H.-W., van der Werf, P. P., de Zeeuw, P. T., & Davies, R. I. 2007, *ApJ*, 671, 1329
- Nowak, N., Saglia, R. P., Thomas, J., Bender, R., Davies, R. I., & Gebhardt, K. 2008, *MNRAS*, 391, 1629
- Noyola, E., Gebhardt, K., Kissler-Patig, M., Lützgendorf, N., Jalali, B., de Zeeuw, P. T., & Baumgardt, H. 2010, *ApJ*, 719, L60

² http://cadwww.hia.nrc.ca/hst/wfpc2/wfpc2_r2.html

- Quataert, E. 2001, in *Astronomical Society of the Pacific Conference Series*, Vol. 224, *Probing the Physics of Active Galactic Nuclei*, ed. B. M. Peterson, R. W. Pogge, & R. S. Polidan, 71–+
- Quillen, A. C., McDonald, C., Alonso-Herrero, A., Lee, A., Shaked, S., Rieke, M. J., & Rieke, G. H. 2001, *ApJ*, 547, 129
- Riffel, R. A., Storchi-Bergmann, T., & McGregor, P. J. 2009, *ApJ*, 698, 1767
- Riffel, R. A., Storchi-Bergmann, T., & Nagar, N. M. 2010, *MNRAS*, 404, 166
- Rose, J. A., Arimoto, N., Caldwell, N., Schiavon, R. P., Vazdekis, A., & Yamada, Y. 2005, *AJ*, 129, 712
- Sellgren, K., McGinn, M. T., Becklin, E. E., & Hall, D. N. 1990, *ApJ*, 359, 112
- Seth, A. C., Blum, R. D., Bastian, N., Caldwell, N., Debattista, V. P., & Puzia, T. H. 2008, *ApJ*, 687, 997
- Seth, A. C. et al. 2010, *ApJ*, 714, 713
- Shapiro, K. L., Cappellari, M., de Zeeuw, T., McDermid, R. M., Gebhardt, K., van den Bosch, R. C. E., & Statler, T. S. 2006, *MNRAS*, 370, 559
- Stolovy, S. R., Hayward, T. L., & Herter, T. 1996, *ApJ*, 470, L45+
- Tonry, J. L. 1984, *ApJ*, 283, L27+
- Ulvestad, J. S., Greene, J. E., & Ho, L. C. 2007, *ApJ*, 661, L151
- van den Bosch, R. C. E., & de Zeeuw, P. T. 2010, *MNRAS*, 401, 1770
- van der Marel, R. P., Cretton, N., de Zeeuw, P. T., & Rix, H. 1998, *ApJ*, 493, 613
- Verolme, E. K. et al. 2002, *MNRAS*, 335, 517
- Walker, M. F. 1962, *ApJ*, 136, 695
- Wallace, L., & Hinkle, K. 1996, *ApJS*, 107, 312
- Winge, C., Storchi-Bergmann, T., Ward, M. J., & Wilson, A. S. 2000, *MNRAS*, 316, 1
- Worthey, G. 2004, *AJ*, 128, 2826
- Zylka, R., Mezger, P. G., Ward-Thompson, D., Duschl, W. J., & Lesch, H. 1995, *A&A*, 297, 83